H-mode access by pellet fuelling in the MAST tokamak

M Valovič, L Garzotti, C Gurl, R Akers, J Harrison, C Michael, G Naylor, R Scannell and the MAST team

EURATOM/CCFE Fusion Association, Culham Science Centre, Abingdon, Oxfordshire OX14 3DB, U. K

E-mail: martin.valovic@ccfe.ac.uk

Abstract. Access into H-mode is studied in the MAST tokamak when plasma is fuelled by cryogenic pellets. It is shown that pellet fuelling from the high field side allows access to H-mode in plasmas heated by neutral beams. Simple and two-stage L-H transitions are identified. The results of comparison of the L-H transitions with pellet injection with transitions where plasmas are fuelled solely by gas puffing depend on the gas puff geometry: Fuelling by high field side gas leads to an L-H transition at the density comparable to the transition with pellet injection. In contrast low field gas can completely prevent the L-H transition.

1. Introduction

H-mode operation at the required density is mandatory for the success of ITER - next step fusion device. However predictions for H-mode access are subject to considerable uncertainty [1] and thus any optimization with respect to the L-H transition is highly relevant. It is well known that to operate in H-mode at given heating power the plasma density should be larger than some threshold value but simultaneously lower than some maximum value. As heating power decreases this density window becomes smaller or in other words the L-H transition diagram - heating power v.s. plasma density - has a minimum. It also is well known that this H-mode density window could be narrowed by a variety of detrimental or unavoidable factors and therefore it is important to identify all possible tools that could act in the opposite direction.

Because plasma density is controlled by the fuelling system it is natural to ask whether the type or geometry of such a system can affect the L-H transition. Any such dependencies could then be explored in order to optimise the H-mode access. There are already indications that such optimization is indeed possible. The dependence of the L-H transition on the location of gas puffing was reported in COMPASS-D [2] and MAST [3]. A favourable effect of pellet fuelling on the L-H threshold was found in DIII-D [4], TUMAN [5] and indicated in MAST [6]. Extension of H-mode to high densities was reported in ASDEX-Upgrade [7]. Although these observations are not yet systematic and not fully understood a reasonable working hypothesis is that the optimum way to fuel the plasma across the L-H threshold is to increase the plasma density inside the separatrix while minimizing the number of particles deposited in scrape-of-layer. High field side pellet fuelling should be then the optimum density control actuator for the L-H transition.

This paper presents data on the L-H transition with pellet fuelling in MAST. It is a continuation of previous studies [4, 5] and expansion of our own observations in [6].

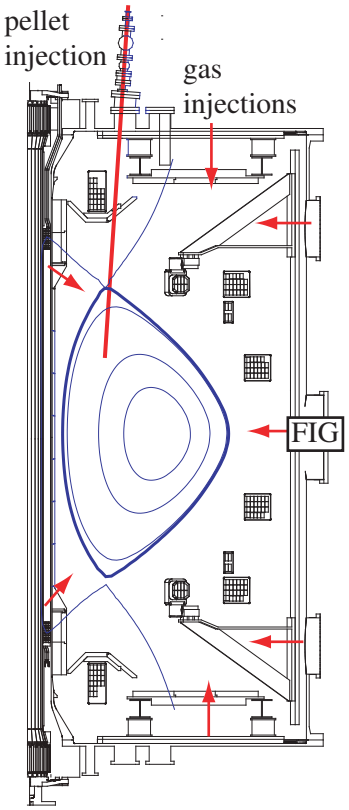

Figure 1. Geometry of fuelling system used. Arrows show the gas fuelling positions. Pellet trajectory and location of fast ion gauge (FIG) are also shown.

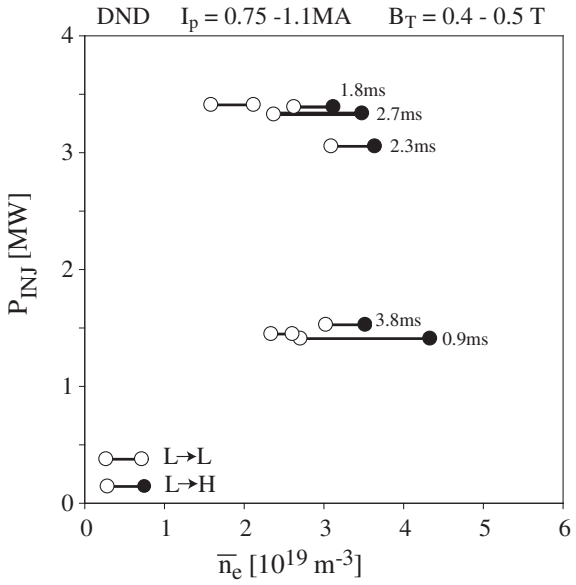

Figure 2. Existence plot for L-H transitions with pellets. P_{INJ} is the injected neutral beam heating power, $\overline{n}_e$ is the line averaged electron density, I_p is the plasma current and B_T is the toroidal magnetic field at the geometric axis.

2. Experimental conditions.

The geometry of the plasma and fuelling systems is shown in Figure 1. The plasma has a double null divertor configuration with major radius $R_{geo} = 0.81m$, minor radius $a = 0.59m$ and elongation $\kappa = 1.9$. In these experiments gas is supplied from 2 high field side (HFS) poloidal locations and five low field side (LFS) poloidal locations. Pellets in these experiments were injected from top-high field side with diameter 1.1-1.7 mm and velocity 240-450m/s. Deuterium was used for both gas puffing and pellets. The plasma was heated by deuterium neutral beams with energy $\leq 65keV$ orientated tangentially in the co-current direction.

The existence diagram of the observed L-H transition with pellet fuelling is shown in figure 2. Each pair of symbols connected with a bar represents a single pellet where symbols show the initial and final density during pellet injection. Pellets which were followed by an L-H transition are shown with a full symbol for post pellet density. The time delay between pellet and L-H transition is indicated next to each symbol. It is seen that transitions occur in a range of neutral heating powers (one and two beam lines). No transition has been recorded with ohmic heating with pellet injection so far. For comparison figure 2 shows also two pellets that were not followed by an L-H transition (open symbol for post pellet density). For these pellets the final density seems to be too low and the pellet

did not lead to an L-H transition. These data indicate that with pellet fuelling there is a density threshold for the L-H transition which is weakly dependent on heating power.

Closer examination of the time histories of available diagnostics reveals that there are two types of L-H transition with pellet fuelling: simple and two-stage transition. There is no correlation between the type of transition and heating power – at each heating power we observe both types of events. The next two sections describe each type in detail.

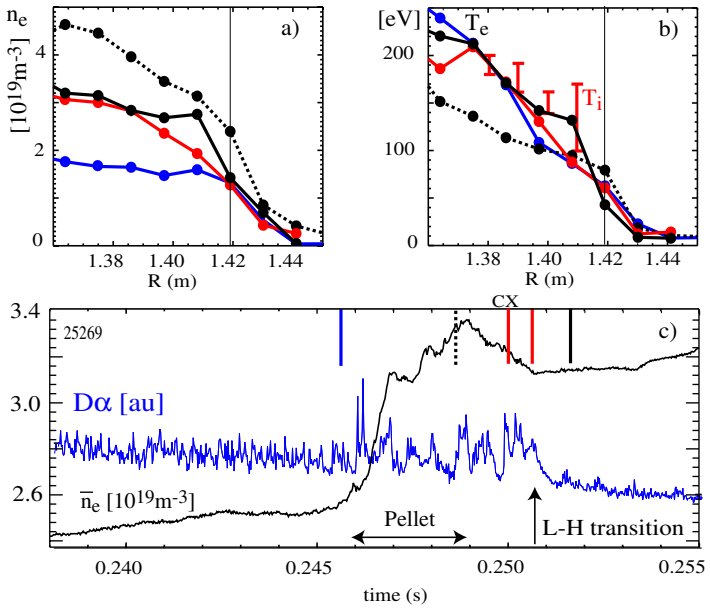

Figure 3. Simple L-H transition. Panel (a): electron density profiles at times indicated in panel (c). Panel (b): full symbols connected with lines are the electron temperature profiles T_e, vertical bars represent the ion temperature profile T_i at time indicated as CX in panel (c). Panel (c): time marks of Thomson scattering and CXRS measurements, $\bar{n}_e$ line averaged electron density, D_α emission intensity. $I_p = 0.9MA$, $B_T(R_{geo}) = 0.49T$, $R_{geo} = 0.82m$, $P_{INJ} = 3.4MW$.

3. Simple L-H transition

In this case the L-H transition occurs a few ms after the pellet is evaporated, without any intermediate stages. An example of such an event is shown in figure 3. From the trace of line averaged density one can identify the time interval during which the pellet is evaporating (indicated as "pellet" in figure 3c). The event-triggered Thomson scattering diagnostic allows measurement of the density profiles just before and just after the pellet evaporation as indicated by time marks in figure 3c. It is seen from figure 3a that the pellet deposited its material on both sides of the separatrix, $R_{sep} = 1.42m$. After the pellet has evaporated, the plasma density rapidly decreases which is consistent with the fact that the plasma is still in L-mode as seen from the D_α emission intensity. The density decay is however not spatially symmetric: the density outside the separatrix reaches the pre-pellet values very quickly while the density inside the separatrix decreases much more slowly and remains always higher than to the pre-pellet values (see the third Thomson scattering profile in Figure 3a). This

difference in density evolution results in a gradual decrease of the density gradient scale length just inside the separatrix. This process culminates in an L-H transition as seen by the drop of D_α emission intensity and change of slope in the trace of $\overline{n}_e$. At the L-H transition the density gradient scale length inside separatrix, $R_{sep} = (1.39 - 1.42)m$, reaches the value of $L_n = \left(\partial \ln n_e / \partial R\right)^{-1} \approx 4cm$. This value is significantly lower than in pre-pellet L-mode. After the L-H transition the density increases as the density pedestal starts to build-up.

The electron temperature does not show any systematic variation as seen in figure 3b. When the pellet is injected the temperature drops but quickly recovers and at the L-H transition is the same as in pre-pellet L-mode. This suggests that the temperature is not a leading control parameter for the L-H transition in these conditions. A similar conclusion was reached for pellet fuelled H-modes in DIII-D [4]. Nevertheless the temperature can a play the role in the L-H transition through the finite Larmor radius effect. Note that at the time of the L-H transition the Larmor radius just inside the separatrix is comparable to the density gradient scale length: $\rho_s = \sqrt{\left(T_e + T_i\right) M_i} / \left(eB_T(R_{sep-})\right) \sim$ $\sim 8mm \sim L_n / 5$. Here the ion temperature is measured by charge exchange resonance spectroscopy (CXRS) at the time point closest to the L-H transition time as indicated in figures 3b and 3c.

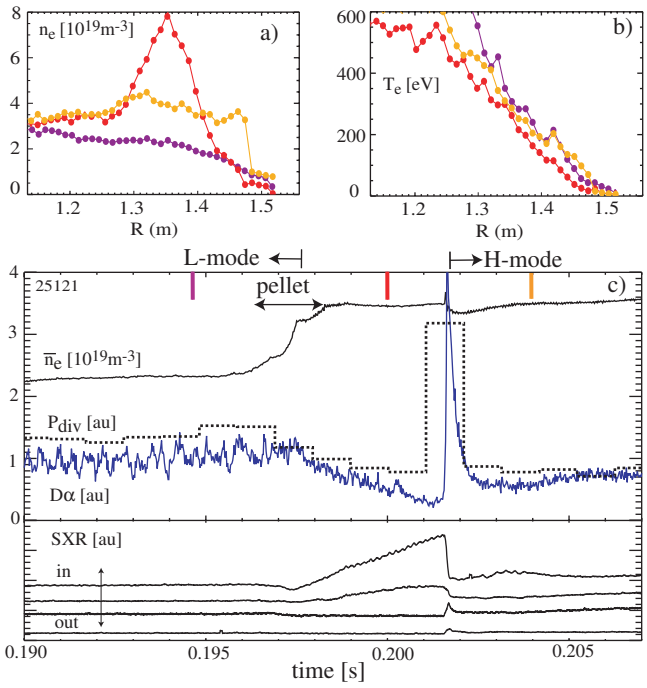

Figure 4. Detail of two-stage L-H transition with pellet fuelling. Panel (a): electron density profiles at times indicated in panel (c). Panel (b): electron temperature profiles T_e at times indicated in panel (c). Panel (c): time marks of Thomson scattering, $\overline{n}_e$ line averaged electron density, D_α emission intensity, P_{div} power to divertor from Langmuir probes and intensities of soft X-rays (SXR). I_p=0.74MA, $B_T(R_{geo}) = 0.40T$, $R_{geo} = 0.87m$, P_{NBI}=3.2MW.

4. Two-stage L-H transition

In this type of event the pellet triggers firstly a phase of improved core confinement, which is short lived, and then is followed by conventional H-mode. This event is shown in figure 4. Immediately after the pellet has evaporated, plasma confinement improves as indicated by a decrease of D_α emission, reduction of power flowing to the divertor and linear increase of more central signals of horizontal SXR camera (see figure 4c). In addition the line averaged density is not decaying as it was in the case of the simple L-H transition. The plasma however is not in conventional H-mode as neither electron density nor electron temperature develop H-mode pedestals (figure 4a and 4b). Such a configuration is not stable and its life time is about 1.8ms. This improved confinement mode is similar to that observed after pellet injection in the limiter tokamak TUMAN [5] including its short lifetime.

The phase described is terminated by a fast event at 0.2016s which causes a fast redistribution of plasma as seen from the density profiles just before and after the event (fig 4a). Signals from the horizontal SXR camera show that this redistribution lasts about $\Delta t_{SXR} \sim 100\mu s$. The redistribution of density is strongly asymmetric (i.e. all material is displaced outwards) indicating a non-diffusive process. Pellet deposited material is transported outwards by approximately $\Delta r \sim 0.1m$. The characteristic radial velocity associated with this redistribution can be estimated as $v_r \sim \Delta r / \Delta t_{SXR} \sim 0.1m/100\mu s \sim 1km/s$. During this redistribution a rather small part $\sim 11\%$ of the pellet deposited material is lost to the divertor. This redistribution is associated with the growth of an MHD instability that can be seen on both SXR and Mirnov signals. Expanded SXR signals reveal an outward propagating structure with a growth time $\sim 10\mu s$ and a life time about the same as the duration of the redistribution process. The toroidal array of Mirnov probes located at the outboard midplane shows that the structure is toroidally asymmetric. The trigger for this instability is unclear but it could be related to increased pressure gradients during the improved confinement after pellet injection.

After the redistribution event described above the plasma promptly enters H-mode with conventional density and temperature pedestals formed as seen in figures 4a and 4b. This phase is followed by conventional ELMy H-mode later on (see fig 5).

5. Pellet-gas comparison

Figure 5 compares L-H transitions with pellet with those using conventional gas puffing. For the pellet case we use the example described in section 4. For gas fuelling cases we use two extreme geometries where gas is applied from the low field side (LFS) and from high field side (HFS) of the plasma respectively. All three discharges have identical plasma current, magnetic field, shape and injected neutral beam power. In all cases the plasma current ramp up phase lasts up to $0.170s$ and during this phase all plasmas are fuelled identically using a combination of LFS and HFS gas puffing. After the ramp up phase different fuelling is applied for each case. At the time of comparison, $t = 0.200 \pm 0.007s$, the plasma's inner and outer radii, and vertical position were controlled within $\delta R_{\min} = 20mm$, $\delta R_{\max} = 5mm$, $\delta z_{mag} = 3mm$, so that small differences in shape are not expected to affect the L-H transition.

It is seen from figure 5 that the plasma fuelled by HFS gas enters the H-mode approximately at the same line averaged density as the target density for pellet fuelled H-mode. However after the L-H transition the density in the gas fuelled plasma is always lower than for the pellet fuelled discharge

despite the same ELM frequency. It has to be noted that the increase of density after the L-H transition is partially limited by the capability of the HFS gas fuelling system.

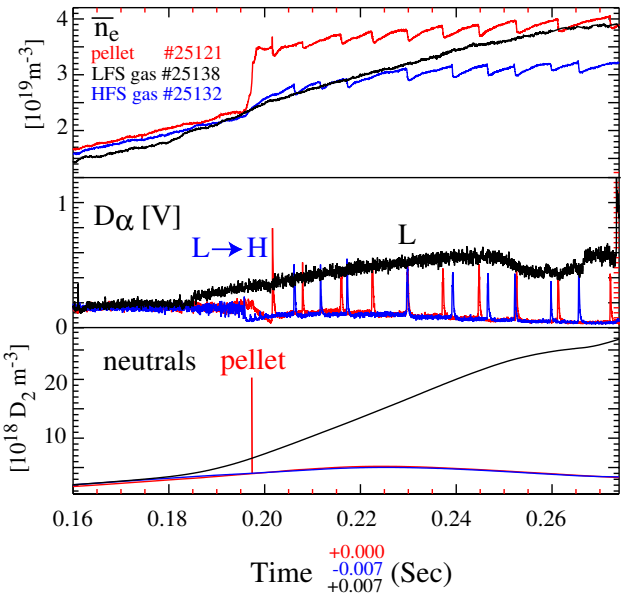

Figure 5. Effect of fuelling method on L-H transition. Top panel: line averaged density, middle panel: D_α emission and lower panel neutral density as measured by a fast ion gauge. For all plasmas: P_{NBI}=3.2MW, I_p=0.74MA, B=0.40T. Note time offsets for shots 25138 and 25132 to align density traces.

Figure 5 also shows a discharge which was fuelled by LFS gas. The gas is applied at 0.180s as seen from the increase of D_α emission and pressure of neutral gas as measured by a fast ion gauge located at the outboard mid-plane (figure 1). (Note that the gauge is sensitive mainly to the gas puffing from LFS valves due to the volume separation by divertor legs.) It is seen that the plasma fuelled by LFS gas remains in L-mode despite the same line average density as the HFS gas discharge at the L-H transition. In addition this plasma remains in L-mode even in later phase where the density is the same as for the pellet fuelled discharge. Inspection of fast video images shows that there are no MARFEs in the LFS gas fuelled plasma. Later on there is an indication of partial detachment of the inner divertor legs (defined as a point where the ion saturation current on the Langmuir probes in the divertor plates is no longer increasing with plasma density). The plasma fuelled by outboard gas has somewhat lower heating power caused by attenuation of the neutral beam due to high neutral pressure. A 1D model shows that the beam attenuation is only 8% at 0.20s and 18% at 0.25s. Therefore the density limit or beam blocking are not reasons for the plasma staying in L-mode.

Examples in figure 5 show that comparison of L-H transitions with pellet and gas fuelling depends on which gas fuelling geometry is used. It also indicates that fuelling can be one of the hidden variables responsible for data scatter in H-mode threshold datasets [1].

6. Conclusions.

We have shown that H-mode can be accessed when plasma is fuelled by high field side pellets. Our data expand previous observations on DIII-D [4], though the database of L-H transitions with pellets remains still sparse compared to gas fuelling. Both DIII-D and MAST data indicate that optimisation of fuelling with respect to H-mode access might be possible. In particular using pellets allows the control of pedestal density independently from the density in the scrape-of-layer which is not possible with gas puff only.

ITER will have a high field side pellet injector [8] which can be used for optimisation of the L-H transition. Pellet deposition in L-mode is not known but it should be somewhat deeper than for H-mode which is predicted to be at the normalised minor radius of $r/a \sim 0.8$ as derived in recent work [9] and in earlier papers [10,11,12]. In our MAST examples the peak of pellet deposited material is the range $r/a = 0.7 - 0.8$ and thus these plasmas are a good model for the ITER situation. The relative pellet size in MAST is larger than in ITER, however if prompt L-H transition by a pellet requires a minimum density perturbation this can be achieved in ITER by increase of pellet injection frequency. Concerning the pellet-gas comparison the situation in ITER should be in between the two extreme cases shown in figure 5 as the main chamber gas puff ring is located at the top-low field side of the ITER vacuum vessel [8]. Finally note that pellets could be a valuable tool also for fast H-mode recovery after an unexpected H-L transition, which is typically associated with a sudden drop of plasma density.

A pellet fuelling system could also be an integral part of MAST upgrade for testing the new extended divertor concept [13]. Firstly pellets might help to decouple the L-H transition (and pedestal in general) from the divertor geometry. Such unfortunate link is often observed in present tokamaks where for example the L-H power threshold depends on position of X-point or on the length of divertor leg [14,15]. A second contribution of pellets could be testing of the divertor under the condition of pellet-induced transients as pellet injection will likely be the main fuelling method in DEMO.

In this paper we are not discussing the possible physics behind the L-H transition with pellets. Here we just note that our results might indicate that the density gradient around the separatrix is one of the important parameters controlling the H-mode access. This assertion seems to be supported by the class of theories based on electron drift waves and inverse cascade which predict that the L-H transition occurs when a certain parameter which is proportional to $1/\sqrt{L_n}$ exceeds a critical value [16,17,18]. In addition increase of edge density gradient in two fluid electromagnetic turbulence simulations, in order to mimic the separatrix, did reproduce many features of the L-H transition [19].

Acknowledgment

This work was funded by the RCUK Energy Programme under grant EP/G003955 and the European Communities under the contract of Association between EURATOM and CCFE. The views and opinions expressed herein do not necessarily reflect those of the European Commission. Drs B Lloyd and D McDonald are gratefully acknowledged for careful reading of the manuscript and valuable comments.

References

[1] Martin Y. *et al* 2008 *J Phys: Conf. Ser.* **123** 012033
[2] Valovič M. *et al* 2002 *Plasma Phys. Control. Fusion* **44** A175
[3] Field A. R. *et al* 2002 *Plasma Phys. Control. Fusion* **44** A113
[4] Gohil P., Baylor L. R., Jernigan T. C., Burrell K. H., Carlstrom T. N. 2001 *Phys. Rev. Lett.* **86** 644
[5] Askinazi L. G. *et al* 1993 *Phys. Fluids* **B5** 2420
[6] Valovič M. *et al* 2008 *Nucl. Fusion* **48** 075006
[7] Lang P. *et al* 38th EPS Conference on Plasma Physics (2011) O3.112
[8] Maruyama S. *et al* 23rd IAEA Fusion Energy Conference, Daejon, Korea, (2010) ITR/P1-28
[9] Garzotti L. *et al* 2012 *Nucl. Fusion* **52** 013002
[10] Polevoi A. R. *et al* 2003 *Nucl. Fusion* **43** 1072
[11] Baylor L. R. *et al* 2007 *Nucl. Fusion* **47** 443
[12] Pégourié B., Köchl F., Nehme H., Polevoi A.R. 2009 *Plasma Phys. Control. Fusion* **51** 124023
[13] Morris A. W. *et al* MAST: Results and Upgrade Activities" 2011 SOFE Conference, Chicago, be published in IEEE transactions
[14] Andrew Y. *et al* 2004 *Plasma Phys. Control. Fusion* **46** A87
[15] Meyer H. *et al* 2008 *Plasma Phys. Control. Fusion* **50** 015005
[16] Rogers B. N., Drake J. F. and Zeiler A. 1998 *Phys. Rev. Lett* **89** 265004
[17] Guzdar P. N., Kleva R. G., Groebner R. J. and Gohil P. 2002 *Phys. Rev. Lett* **89** 265004
[18] Fundamenski W., Militello F., Moulton D., McDonald D. C. 2011 submitted to *Plasma Phys. Contr. Fusion*
[19] A. Thyagaraja, M. Valovič, and P. J. Knight 2010 *Phys. Plasmas* **17** 042507